

Multimode-Floquet-Polariton Superradiance

Christian H. Johansen,^{*} Johannes Lang,[†] and Francesco Piazza[‡]
Max-Planck-Institut für Physik komplexer Systeme, 01187 Dresden, Germany

We consider an ensemble of ultracold bosonic atoms within a near-planar cavity, driven by a far detuned laser whose phase is modulated at a frequency comparable to the transverse cavity mode spacing. We show that a strong, dispersive atom-photon coupling can be reached for many transverse cavity modes at once. The resulting Floquet polaritons involve a superposition of a set of cavity modes with a density excitation of the atomic cloud. We show that their mutual interactions lead to distinct avoided crossings between the polaritons. Increasing the laser drive intensity, a low-lying multimode Floquet polariton softens and eventually becomes undamped, corresponding to the transition to a superradiant, self-organized phase. We demonstrate the stability of the stationary state for a broad range of parameters, including modulation frequencies larger than the separation between transverse cavity modes.

I. INTRODUCTION

The implementation of strong interactions between photons mediated by a medium [1] is essential for quantum-information processing [2, 3], and at the same time allows for the exploration of the quantum many-body physics of light [4, 5]. Photons inherit interactions from the material through the formation of polaritons [6], hybrid quasiparticles corresponding to an excitation present both in the electromagnetic field and in the material.

The creation of interacting polaritons having access to a macroscopic number of modes is essential for the study of thermodynamic phases of photons and complex types of order [4, 5, 7–15]. The strong-coupling between matter and light, required to implement photon interactions, can be realized by reducing the electromagnetic-mode volume using optical cavities or evanescent fields [1]. The former can also be combined with the use of Rydberg atoms to further enhance interactions [16]. This task obviously becomes more challenging if it needs to be achieved for a whole set of electromagnetic modes, which are in general separated in frequency. One solution is to shape the cavity geometry such that a set of quasidegenerate modes is formed [4, 17–19]. Another option is to use a set of propagating modes as in cavity arrays [14] or photonic crystals [20].

An alternative route towards interacting multimode polaritons has been recently demonstrated experimentally via Floquet engineering of Rydberg levels in a non-degenerate optical cavity [21]. Starting from a given atomic transition resonantly coupled to a single cavity mode, the periodic amplitude modulation of the laser dressing effectively splits the transition into multiple levels separated by the modulation frequency, one of them becoming resonant with a second cavity mode. The resulting two-mode polaritons strongly interact via the Ry-

dberg component inherited from the atomic levels. This demonstrated the potential to Floquet engineer interacting multimode polaritons for the exploration of the many-body physics of light.

In this work, adopting similar ideas, we theoretically study a first example of a phase transition to an ordered phase emerging for multimode Floquet polaritons. Differently from the setup used in [21], the realization of polaritons and their interactions is achieved here via the dispersive coupling between the motional degrees of freedom of an ultracold Bose gas and the transverse electromagnetic (TEM) modes of a near-planar Fabry-Perot resonator [22, 23], with mode-spacing in the GHz range. Similarly to the case of plasmon-polaritons in electronic matter [24], here the polaritons mix a cavity-photon with a density excitation in the gas of neutral atoms.

If performed at a frequency close to the TEM mode-spacing, a periodic phase modulation of the laser can bring a large number of modes into resonance. This is achieved without heating the atoms, since ultracold density excitations are in the kHz range, and the internal dynamics can be at hundreds of GHz for a correspondingly detuned laser. The mutual interactions between multimode Floquet polaritons induce avoided crossings, controlled not only by the effective light-matter coupling and detunings, but also by the phase-modulation amplitude. As a consequence, a low-lying multimode Floquet polariton can be red-shifted to zero frequency and subsequently become undamped, corresponding to an instability towards a multimode superradiant phase with macroscopic occupation of the polariton.

The observation of the avoided crossings between interacting Floquet polaritons requires sub-recoil resolution achievable in long cavities [23]. Using ultracold bosons coupled to such cavities, single-mode superradiance has already been observed [25], and Floquet modulation has also been studied, but at frequencies far below the transverse mode spacing [26, 27].

Multimode superradiance has been recently observed using ultracold bosons coupled to degenerate confocal resonators [28–31], and is expected to give access to beyond-mean-field effects due to the increased locality of the light-matter coupling [32, 33]. On the other hand,

^{*} chj@pks.mpg.de

[†] gu53jup@pks.mpg.de

[‡] piazza@pks.mpg.de

Floquet superradiance has so far only been studied in the single-cavity-mode case. Here we show that one can enter the deep multimode regime even in near-planar cavities.

II. THEORETICAL DESCRIPTION

A. Model

We consider a cloud of bosonic atoms trapped inside a near-planar optical cavity and transversally pumped by a laser, as depicted in Fig. 1. This laser is phase modulated (PM) with a frequency comparable to the energy difference between the TEM modes of the cavity. The pump laser is described as a classical field

$$E(t, \mathbf{x}) = 2\lambda \eta_p(\mathbf{x}) \cos(\omega_p t + f(t)), \quad (1)$$

with ω_p being the carrier frequency of the pump and η_p its spatial profile. The PM function, $f(t)$, is assumed to be periodic $f(t+T) = f(t)$ and real. Because of the periodicity one can represent $e^{-if(t)}$ as a discrete Fourier series

$$e^{-if(t)} = \sum_{\alpha=-\infty}^{\infty} c_{\alpha} e^{-i\alpha\Omega t}, \quad (2)$$

where $\Omega = \frac{2\pi}{T}$. In experiments the PM is generated using an electro-optic modulator with a limited bandwidth. We therefore consider a series with finite support and define α_M as the index where the sum can be truncated, $c_{|\alpha|>\alpha_M} \sim 0$. The carrier frequency of the pump is red detuned from the atomic transition ω_e , in such a way that the detuning between atoms and pump Δ_a , satisfies $\Delta_a = \omega_e - \omega_p \ll \omega_e + \omega_p$. For instance, for ^{87}Rb atoms, the $S_{1/2} \rightarrow P_{1/2}$ transition has a frequency $\omega_e \approx 378$ THz [34]. In that case $\Delta_a \sim 10^2$ GHz will easily satisfy the inequality. Similarly, the PM frequency is chosen to be much smaller than Δ_a , such that $\Delta_a + \alpha_M \Omega \sim \Delta_a$. Due to this condition it is well justified to apply the rotating wave approximation [35].

Since Δ_a is large compared to the inverse lifetime of the excited state, the occupation of the latter remains small and saturation effects are negligible. Therefore, the ground and excited states of the atoms can be represented as two independent bosonic fields. The resulting Hamiltonian, in the frame rotating with the carrier frequency, in units where $\hbar = 1$, reads

$$\begin{aligned} H = \int d\mathbf{r} \left\{ \psi^\dagger \left(-\frac{\nabla^2}{2m} + V_g(\mathbf{r}) \right) \psi + \phi^\dagger \Delta_a \phi \right. \\ \left. + \phi^\dagger \left(\sum_i g_i \eta_i(\mathbf{r}) a_i + \lambda \eta_p(\mathbf{r}) e^{-if(t)} \right) \psi + \text{H.c.} \right. \\ \left. + \sum_i \Delta_i a_i^\dagger a_i \right\}. \end{aligned} \quad (3)$$

Here ψ (ϕ) is the bosonic annihilation field operator for the ground (excited)-state of the atoms with mass

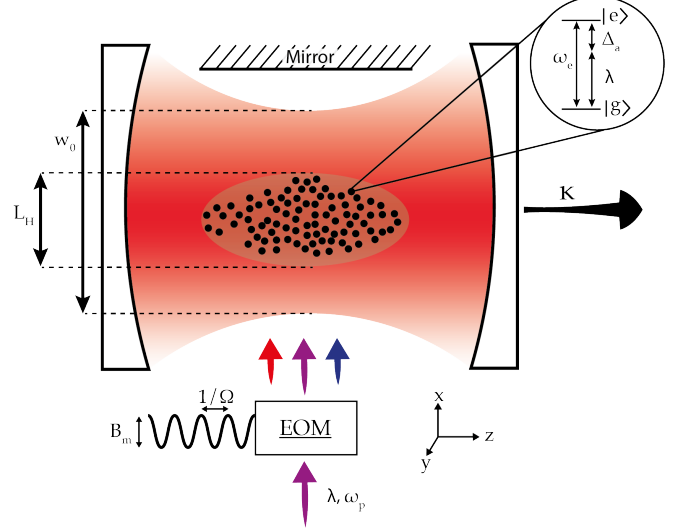


FIG. 1: The physical setup considered, consists of a linear cavity with a waist of w_0 . Inside the cavity ultracold bosonic atoms are confined within a cigar-shaped harmonic trap, with a transverse harmonic oscillator length of L_H . Each atom is modelled as a two-level system with excited-state energy ω_e . The atoms are transversally pumped with a laser of frequency ω_p and pump strength λ . The laser is sent through an electro-optical modulator which introduces a periodic phase-modulation with period $1/\Omega$ and depth B_m . Photons are lost from the cavity mirrors with rate κ , making the system driven-dissipative.

m . The space-time dependence of field operators has been suppressed for brevity. As Δ_a is much larger than both kinetic and trapping energy of the excited state, these terms have been neglected. $\eta_j(r)$ is the spatial mode function for the j 'th cavity mode that couples with strength g_j to the atoms. The j 'th transverse cavity mode has detuning $\Delta_j = \omega_j - \omega_p$ and is annihilated by the bosonic operator a_j . We consider the case where higher-order cavity modes have an approximate linear energy spacing $\Delta_j \approx \Delta_0 + j\omega_T$. Choosing a PM frequency Ω that is comparable to ω_T means that the detuning between higher-order modes and the atomic transition can be compensated by coupling to the higher frequency pump sidebands, generated by the PM. As the PM is periodic, the sidebands are equidistant in frequency, separated by Ω .

All modes couple to all sidebands but the coupling is inversely proportional to the detuning. Because Ω is large the only relevant modes are the near-resonant ones

$$\Delta_i \pm \alpha\Omega \sim \Delta_0. \quad (4)$$

The cavity is an intrinsically lossy system, which compensates the energy input from the continuous pumping. This loss is included by coupling the cavity to a continuum of electromagnetic modes playing the role of a bath [36]. At optical frequencies the electromagnetic bath is

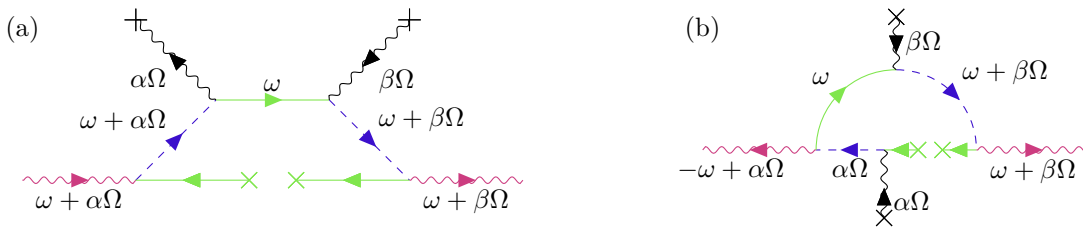


FIG. 2: The scattering processes that determine the polarizability of a BEC driven by a PM laser. In these Feynman diagrams, the straight (wavy) lines represent propagation of a bare atom (photon) labeled by its frequency. The momentum/mode indices have been suppressed for brevity. Green lines represent atoms in the electronic ground state and blue dashed ones atoms in the excited state. The purple wavy line represent cavity photons. In addition, there are external sources, represented by lines ending in a cross. Those can be photons from a given sideband of the phase-modulated laser (see discussion in section II A), depicted as a black wavy line, or atoms from the BEC, depicted as solid green lines. Panel a) shows the normal process, whereas panel b) shows the anomalous process where the laser acts as a false vacuum.

effectively at zero temperature and is therefore well described as a Markovian loss for the photons. This means that in the von Neumann equation

$$\frac{d\rho}{dt} = -\frac{i}{\hbar} [H, \rho] + D\rho, \quad (5)$$

the unitary Hamiltonian term is supplemented with a Lindblad dissipator [36]

$$D\rho = -\sum_j \kappa_j \left(\frac{1}{2} \{a_j^\dagger a_j, \rho\} - 2a_j \rho a_j^\dagger \right). \quad (6)$$

This Markovian modeling of the environment is also valid when the PM is included, as long as the environment spectral function appears flat over the energy range $\omega_p \pm \alpha_M \Omega$.

As usual, the atom number is assumed to be constant over the duration of the experiment. By coupling the atoms to the cavity the total energy, on the other hand, is not conserved. In the regime where the cavity-mode detunings are comparable to the recoil energy $\epsilon_r = Q^2/(2m)$, this leads to a non-thermal state of the bosonic atoms [37]. In the following, we will neglect this effect by assuming that the time τ_{rel} required to reach that state is longer than the experimental time, which is realistic for sufficiently large detunings and trap sizes, since τ_{rel} scales inversely with these quantities [37]. We will therefore assume the atoms to be initially cooled down to an ultracold temperature T much smaller than the recoil energy, so that thermal excitations are of little concern and we can model the atoms as a perfect BEC.

B. Polarizability of the Floquet-driven bosonic gas

Collective polaritonic excitations correspond to the normal modes of the electromagnetic field including polarization effects, that is, the modification of the propagation of light due to the medium. In our case, the latter is a gas of ultracold bosonic atoms, whose internal electronic transition is driven by a PM laser, as described in

section II A. The assumption that the bosons are initially in a perfect BEC at zero temperature corresponds to all atoms being in the electronic ground state and also in the lowest motional state.

The effect of this driven, polarizable medium on the cavity photons is depicted in Fig. 2, where we illustrate the relevant scattering processes. In Fig. 2 (a), a cavity photon excites an atom out of the BEC, and takes it to an electronically and motionally excited state (see second line in Eq. (3)). The atom then emits a photon into the laser and returns back to its electronic ground state and at a momentum which does not belong to the BEC (otherwise the net effect of the whole process would not contribute to the polarizability). The whole sequence is then repeated backwards, leading to the emission of a photon back into the cavity.

The motional scales of cold atoms are in the kHz range while the considered PM frequencies are comparable to the TEM mode spacing, which is of the order of GHz. The scattering process is therefore significantly suppressed if the incoming cavity photon excites the atomic ground state to energies which are large compared to the recoil energy, unless excess is compensated by the laser. With a single laser frequency this is impossible, which leads back to a single-mode scenario. However, via PM the laser sidebands can be brought close to resonance with the high-energy modes. In the formalism this can be efficiently accounted for by splitting the energy (ω') into Floquet sectors $\omega' = \omega \pm \alpha\Omega$, where $\omega \in \{-\Omega/2, \Omega/2\}$ is the quasienergy. In the diagrams of Fig. 2, this means that if a photon at energy $\omega + \alpha\Omega$ excites the atoms, then the laser has to remove an energy $\alpha\Omega$ for the process to be non-negligible.

The same scattering process can clearly also take place with the role of cavity and laser being exchanged, which corresponds to the anomalous process [38, 39] depicted in Fig. 2 (b), where the laser plays the role of a false vacuum.

The crucial point is that, in all these processes, due to the periodic PM of the driving laser, the initial and the final cavity photon can have different frequencies without the atomic ground state propagating at a high energy and

thus far off-shell. Due to the absorption and emission of laser photons from different sidebands the polarizability of such a Floquet-driven BEC is thus not diagonal in frequency space as it couples different Floquet sectors of the cavity field differing by multiples of Ω .

Under the condition, stated in section II A, that the highest sideband of the laser is still far detuned from the electronic transition, one can adiabatically eliminate the electronic excited state from the diagrams in Fig. 2. This leads to the following dynamical polarizability:

$$\chi_{i,j;\alpha,\beta}(\omega) = \Lambda^2 \bar{c}_\alpha c_\beta \Pi_{i,j}^R(\omega), \quad (7)$$

which has been expressed as a matrix in the TEM-mode basis, with indices i, j , and in the Floquet basis, denoted by α, β . Here we also introduced a single parameter, the effective light-matter coupling strength $\Lambda = \lambda g \sqrt{N_0} / \Delta_a$, which increases linearly with the pump strength. This can be captured in a single parameter because the energetic difference between the transverse modes is on the order of GHz while the total energy in the electric field is hundreds of THz [40]. This justifies approximating all modes to have a similar coupling to the atoms ($g_i = g$).

Again due to the large energy difference between the atomic ground-state motion and the PM frequency Ω the density response, Π^R in Eq. (7), is diagonal in frequency, and takes the form of a bosonic analog of the Lindhard function [41], which specified for a perfect BEC in a trap [38] reads

$$\Pi_{i,j}^R(\omega) = \sum_n \frac{-2(\epsilon_r + \epsilon_n)}{(\omega + i0^+)^2 - (\epsilon_r + \epsilon_n)^2} \times \langle \psi_0 | \eta_j \eta_p | \psi_n \rangle \langle \psi_n | \eta_i \eta_p | \psi_0 \rangle, \quad (8)$$

where ϵ_n is the energy of the atomic transverse modes and we have assumed that the wave functions of the cavity modes, as well as those of the atomic eigenstates, are real.

In summary, we see that in this regime the non-diagonal frequency structure of the polarizability, coupling two different Floquet sectors α, β , is simply encoded in the product of two Fourier coefficients $c_\alpha c_\beta$ of the periodic modulation of the laser phase. Each coefficient quantifies how much of the laser intensity goes into the corresponding sideband i.e. how strong that sideband couples to the electronic transition. According to the process shown in Fig. 2, these weights clearly have to enter the polarizability. The remaining part of the polarizability is then given by the retarded density response of the medium, which only depends on the low energy motional degree of freedom of the atoms in their electronic ground state.

The physical content of the density-response function is quite transparent: it features the matrix element of the transition from the trap ground state $|\psi_0\rangle$ to an excited state $|\psi_n\rangle$, and back to the ground state. The transition out of (back to) the ground state is induced by the spatially-varying optical potential $\eta_i \eta_p$ ($\eta_j \eta_p$), created by the interference between the laser and the cavity field of

the i 'th (j 'th) TEM mode. As it is clear from inspection of the matrix elements, for a generic choice of the atom trap, the density response, and in turn the polarizability, need not be diagonal in the cavity-mode basis.

In summary, the Floquet-driven bosonic medium can change both the frequency (by multiples of the modulation frequency Ω) and the TEM mode of an incoming photon. Whether and how this happens depends on the specific choice of the PM of the laser, the cavity geometry and the trapping potential for the atoms, as we discuss next.

1. Symmetric trap and harmonic phase modulation

We consider the radially symmetric configuration of a cigar-shaped harmonic trap in the center of a near-planar cavity. Assuming a long cigar-shaped zero-temperature BEC the longitudinal wave function is well localized in momentum space with a negligible width $\Delta k \ll Q$. Upon absorption of a photon the atoms therefore scatter into a state with longitudinal momentum Q and recoil energy ϵ_r .

Assuming that the laser wavelength, λ_p , is much smaller than the transverse diameter of the BEC L_H , means that the pump oscillates many times over the size of the cloud. The transverse spatial modes of the atoms then satisfies a Mathieu equation with an additional quadratic term. The momentum kicks associated with the laser oscillation leads to far off-shell processes which can be neglected, unless the kicks during one scattering process, Fig. 2, cancels out. As the cavity mode functions are considered larger than the atom cloud the fast oscillations of the Mathieu equation can be neglected and the radially symmetric trap determines the BEC shape. Following these considerations, we can simplify the pump mode function as a constant, $\eta_p = 1$. When this approximation is not valid, the pump breaks the radial symmetry of the trap and introduces periodic modulations along the laser axis, which requires the full numerical solution of the modified Mathieu equation.

For a small λ_p , the transverse modes which we seek to couple are Laguerre-Gauss (LG) modes, which for the cavity read [42]

$$\text{LG}_{jp}(r, \Theta) = \frac{e^{-r^2/2w_0^2 + ip\Theta} \sqrt{\frac{j!}{(p+j)!}} \left(\frac{r}{w_0}\right)^{|p|} L_j^{|p|} \left(\frac{r^2}{w_0^2}\right)}{w_0}, \quad (9)$$

with $L_j^{|p|}(x)$ being the associated Laguerre polynomial of order j . The ground-state atoms have similar mode functions but with w_0 replaced by L_H .

For atom clouds that are radially symmetric around the cavity axis, angular momentum conservation implies that for each overlap the angular index must be conserved. The BEC is in the ground state with zero angular momentum and therefore only radial cavity modes with the same absolute angular momentum are coupled. Hav-

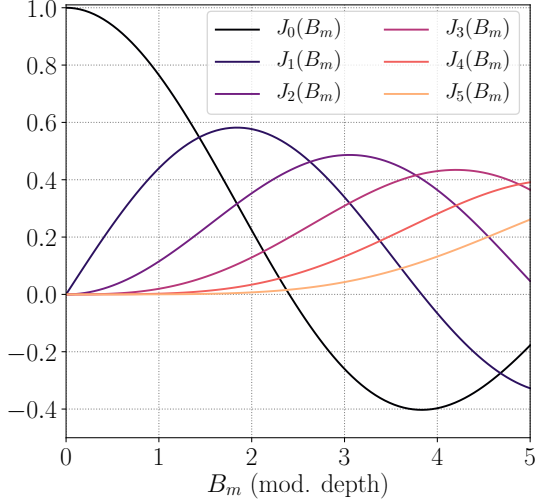


FIG. 3: A plot of the first six phase-modulation coefficients as a function of the modulation amplitude. The coefficients are given by the Bessel functions of the first kind.

ing the carrier frequency being only slightly detuned from the zeroth TEM mode means that only cavity modes with $p=0$ are relevant and thus $\eta_j(x) = w_0 \text{LG}_{j0}(r) \cos(Qz)$, rendering all mode functions and eigenstates in the density response function real. The remaining radial overlap has a closed form solution shown in appendix A. The simplest case is when the BEC is significantly narrower than the cavity waist. In this case all overlaps are negligible except the one with the atomic state in the zeroth radial mode and a longitudinal momentum given by the recoil momentum. In this case, the density response takes a simple form

$$\Pi_{i,j}^R(\omega) = \frac{-2\epsilon_r}{(\omega + i0^+)^2 - \epsilon_r^2}, \quad (10)$$

which is the same as the single mode result [38].

For non-zero modulation depth it is necessary to parametrize the PM, which can be any real function that is periodic in time. A simple yet flexible choice is a harmonic modulation:

$$f(t) = B_m \sin(\Omega t),$$

with the amplitude B_m being a real number. From the Jacobi-Anger expansion [43], the discrete Fourier coefficients are known to be Bessel functions of the first kind $e^{if(t)} = \sum_{\alpha} c_{\alpha} e^{i\alpha\Omega t}$, with $c_{\alpha} = J_{\alpha}(B_m)$. As shown in Fig. 3, for zero modulation depth, the zeroth-order coefficient is the only non-zero component, which is exactly equivalent to having no PM. Because of the orthonormal nature of the coefficients, the weight in the zeroth-order component is distributed as the modulation is increased. As discussed in section II B, since the coefficients directly determine how strongly different modes are coupled by

the medium, one can tune the amount of multimodality to a large extent by simply changing the modulation depth.

The modulation frequency Ω is equally important, as it determines the effective detunings of the different cavity modes. If the modes are exactly linearly spaced one can make the system energetically degenerate by choosing Ω equal to the mode spacing. If one wants to energetically suppress either higher or lower order modes, one can choose a frequency that is either smaller or greater than the mode spacing. Thus, even though the specified harmonic modulation has only two parameters, it is nevertheless highly tunable.

III. MULTIMODE FLOQUET POLARITONS

Having determined the polarizability of the Floquet-driven BEC, we can now investigate how this modifies the propagation of cavity photons and leads to the formation of polaritons. As already mentioned above, polaritons are the normal modes of the electromagnetic field inside the medium. As such, they appear as poles of the Green's function of the electromagnetic field. In the present case, this Green's function reads

$$\mathcal{D}_{i,j;\alpha,\beta}^R(\omega) = \begin{pmatrix} P_{i,j;\alpha,\beta}^R(\omega) + \chi_{i,j;\alpha,\beta}(\omega) & \chi_{i,j;\alpha,\beta}(\omega) \\ \chi_{i,j;\alpha,\beta}(\omega) & P_{i,j;\alpha,\beta}^A(-\omega) + \chi_{i,j;\alpha,\beta}(\omega) \end{pmatrix}^{-1}, \quad (11)$$

where the positive- and negative-frequency components of the electromagnetic field have been separated. The resulting Nambu matrix depends on the inverse Green's function of the bare cavity

$$P_{i,j,\alpha,\beta}^{R/A}(\omega) = \delta_{i,j} \delta_{\alpha,\beta} (\omega - \Delta_j - \alpha\Omega \pm i\kappa_j),$$

where R/A indicate the causality of the Green's function being retarded or advanced. This combination of Green's function appears here because both positive and negative frequencies are present.

Due to the polarization function in Eq. (11), the Green's function of the electromagnetic field is non-diagonal in both frequency and LG-mode space, such that its computation, in general, becomes rather cumbersome. However, as long as the polarizability decays on an energy scale much smaller than $\Omega \sim \omega_T$, the calculations allow for simplifications. In this case the cavity modes that actually contribute to the electromagnetic Green's function are the ones that are near-resonant modulo a multiple of the modulation frequency: $\Delta_i + \alpha\Omega \sim \Delta_0$. This effectively couples the sideband α with the mode index i , largely reducing the number of elements of the matrix in Eq. (11).

In order to visualize the poles of the electromagnetic Green's function, we will use the so-called spectral func-

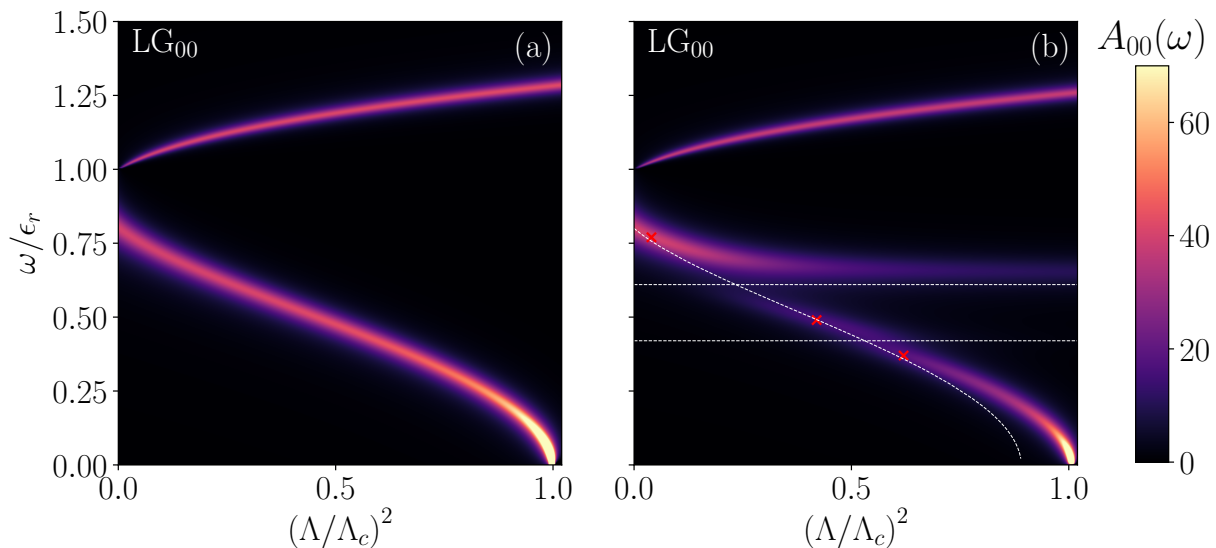


FIG. 4: Distribution of the spectral weight in the LG_{00} -component of the cavity field. a) when no phase-modulation is applied to the laser, $B_m = 0$ and b) when $B_m = 0.9$, $\Omega = (\omega_T + 0.19)\epsilon_r$. The remaining parameters are $\Delta_0 = 0.8\epsilon_r$, $w_0/Q = 200$, $L_H = 10^{-3}w_0$ and $\kappa = 0.02\epsilon_r$ with the parameters described in section II B 1. The horizontal dashed lines in b) represent the effective detunings of higher order modes, while the decreasing dashed line represents the position of the spectral line from a). The three red crosses mark the values used in Fig. 5.

tion of the cavity

$$A_{ij;\alpha\beta} = i \left(\mathcal{D}_{ij;\alpha\beta}^R - [\mathcal{D}_{ji;\beta\alpha}^R]^\dagger \right). \quad (12)$$

This function has peaks in correspondence to the real part of the poles (the polariton frequency), with a width set by the imaginary part (the polariton damping or inverse lifetime). The features observed in the spectral function can be measured by pump-probe or transmission experiments.

A. No phase-modulation

To put our results into perspective and highlight effects of the coupling between many cavity modes, we first review some features of the single-mode calculation [38, 44]. The spectral function for the unmodulated cavity is shown in Fig. 4 (a). When the cavity couples weakly to the atoms the cavity spectrum is dominated by the free Lorentzian peak centered at the detuning Δ_0 with a width determined by the cavity loss κ . As the pump strength is increased the atoms start to hybridize with the cavity. This leads to a second peak in the cavity spectral function initially at the recoil frequency, corresponding to the characteristic energy of the xdensity excitation in the atoms. This signature is initially extremely narrow but broadens as the pump strength is increased. In addition, the repulsion between the hybridized modes is also continuously increasing, thereby moving away from the bare resonances. This repulsion between the cavity and atomic peaks signals appreciable

hybridization i.e. mixed atom-photon character of the polaritons.

By increasing the coupling Λ , the low-lying polariton is pushed to lower and lower energies until its frequency reaches zero. At this point, its damping is still finite and the peak in the spectral function is no longer Lorentzian [37, 38]. By further increasing the coupling to a critical value Λ_c , also the polariton damping vanishes and the normal phase becomes unstable. In the current parameter regime where only the lowest-order atomic transverse-mode is relevant, the critical coupling strength Λ_c can be found analytically [45]

$$\Lambda_c^2 = \frac{\kappa^2 + \Delta_0^2}{4\Delta_0} \epsilon_r. \quad (13)$$

If the cavity loss is significantly smaller than the detuning, then Λ_c is approximately linearly dependent on Δ_0 .

B. Including phase-modulation

Considering the same system, but turning on the phase modulation, more cavity modes can be brought into play. How strongly these couple to the atoms is determined by the modulation depth according to Eq. (7). As seen in section II B 1, for small atom clouds the density response becomes independent of the mode index, that is the spatial structure of the LG_{j0} cavity modes plays no role in determining how strongly they couple. Therefore, assuming that they have similar detunings (modulo the PM frequency Ω), the cavity mode admixture is fully determined by the PM of the laser. This allows one to

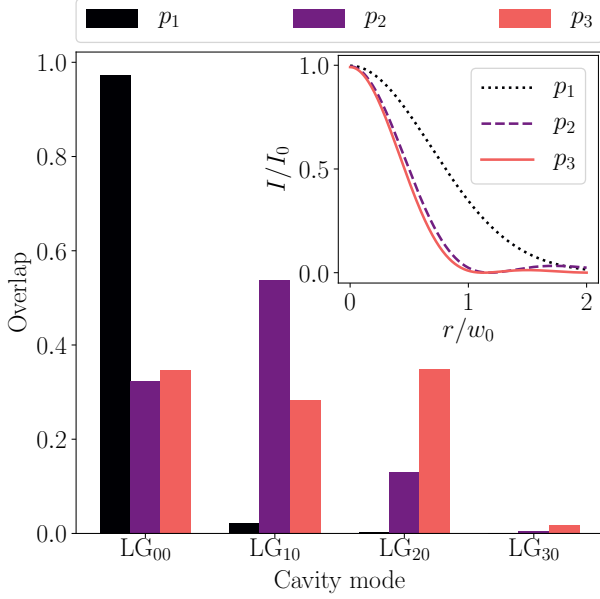


FIG. 5: The overlap of different LG modes with the total cavity field at the three points marked by red crosses in Fig. 4 (b): $p_1 = (0.04, 0.77)$, $p_2 = (0.42, 0.49)$, $p_3 = (0.62, 0.37)$. The inset shows the resulting total radially symmetric mode profiles in real space.

create polaritons with a photonic part consisting of a superposition of several cavity modes.

When multiple cavity modes are available, the photon Green's function is a matrix in the cavity-mode basis (see Eq. (11)). As argued above, for the parameters considered here, the matrix structure in the Floquet basis can be suppressed since its index is fixed by the cavity mode, i.e. the Green's function in Eq. (11) is proportional to $\delta_{i\alpha}\delta_{j\beta}$. The spectral function is thus also a matrix in the cavity-mode basis. In order to illustrate the effect of the PM, we show the diagonal entry of the spectral function corresponding to the LG₀₀ mode in Fig. 4 (b). This allows a direct comparison with the unmodulated case of Fig. 4 (a). Using a PM frequency of the form $\Omega = \omega_T + \epsilon$, the effective detunings of the higher-order modes become

$$\Delta_i = \Delta_0 - \epsilon. \quad (14)$$

Choosing the sign of ϵ allows one to switch between cases where higher-order modes are effectively lower or higher in frequency than the zeroth mode.

For the spectral function plotted in Fig. 4 (b), ϵ is chosen to be a small positive number, which causes the higher order modes to be energetically preferred. With a weak modulation depth ($B_m = 0.9$) the only new relevant modes are LG₁₀ and LG₂₀, which are given by Eq. (9). The magnitude of the pump-sidebands, generated by the PM, is given by the corresponding Fourier coefficient squared. The effective light-matter coupling

strength between each mode and the atoms is therefore given by the Fourier coefficient of the nearest sideband (Fig. 3). The relevance of each mode is determined by its atom-coupling strength and the magnitude of the effective detuning. For the specific case of the figure, this means that the LG_{j0} mode couples only to the j 'th sideband, which has a magnitude of $J_j(B_m)^2$. Coupling to all the other sidebands leads to far detuned processes with very small magnitudes.

A first clear signature of the multimode nature is the appearance of more peaks in the spectral function. Looking at Fig. 3 at $B_m = 0.9$ one sees that the zeroth mode has the largest coupling to the atoms. This means that at small Λ this mode is the only contribution seen. As Λ is increased, LG₁₀ starts having a non-negligible coupling to the atoms. Because this mode is ϵ closer to its sideband than LG₀₀ is to the carrier frequency, LG₁₀ becomes more favourable for the system and one observes a clear avoided crossing near the frequency of the bare LG₁₀-mode. This repeats when the LG₂₀ starts being relevant and a second avoided crossing is observed at Δ_2 .

These avoided crossings signal the strong hybridization between cavity modes and the emergence of multimode Floquet polaritons. This is confirmed by Fig. 5, where the overlap of the LG modes with the total cavity field is shown for different points on the polariton branches of Fig. 4 (b). This also explicitly demonstrates that the LG₃₀ can be neglected as presumed based on its coefficient in Fig. 3. In the inset of Fig. 5 the resulting mode profile of the total cavity field is shown. Already for the few modes involved here, it is clearly seen that the PM leads to a significant decrease of the waist of the cavity field, which is bounded from below by the central waist for the highest involved TEM mode. The observed reduction of the waist of the cavity field directly implies a reduction of the range of the cavity-mediated interactions [29]. More prominent effects can obviously be achieved by increasing the PM amplitude, but also by displacing the atom cloud from the center of the cavity. The oscillating nature of higher-order transverse modes can then lead to interference effects that further decrease the interaction range.

Changing the modulation depth B_m gives the freedom to choose how strongly the different modes couple to the atoms. The parameters B_m and ϵ are completely independent and therefore allow one to tune between a wide range of different multimode scenarios. In Fig. 4 (b) we showed how choosing $\epsilon > 0$ leads to avoided crossings due to the higher-order modes being energetically favoured. In Fig. 6 we choose $\epsilon < 0$ which means the zeroth mode is always energetically most preferable. The ratio $\Lambda/\Lambda_c = 0.7$ is kept fixed for all modulation amplitudes, while the latter is varied over a range where only the first four modes are relevant. In order to facilitate the visualization of the avoided crossings, the approximate polariton frequencies are overlaid as red-dashed lines.

Consider first the case of no modulation ($B_m = 0$). The LG₀₀ mode's spectral function shows the familiar

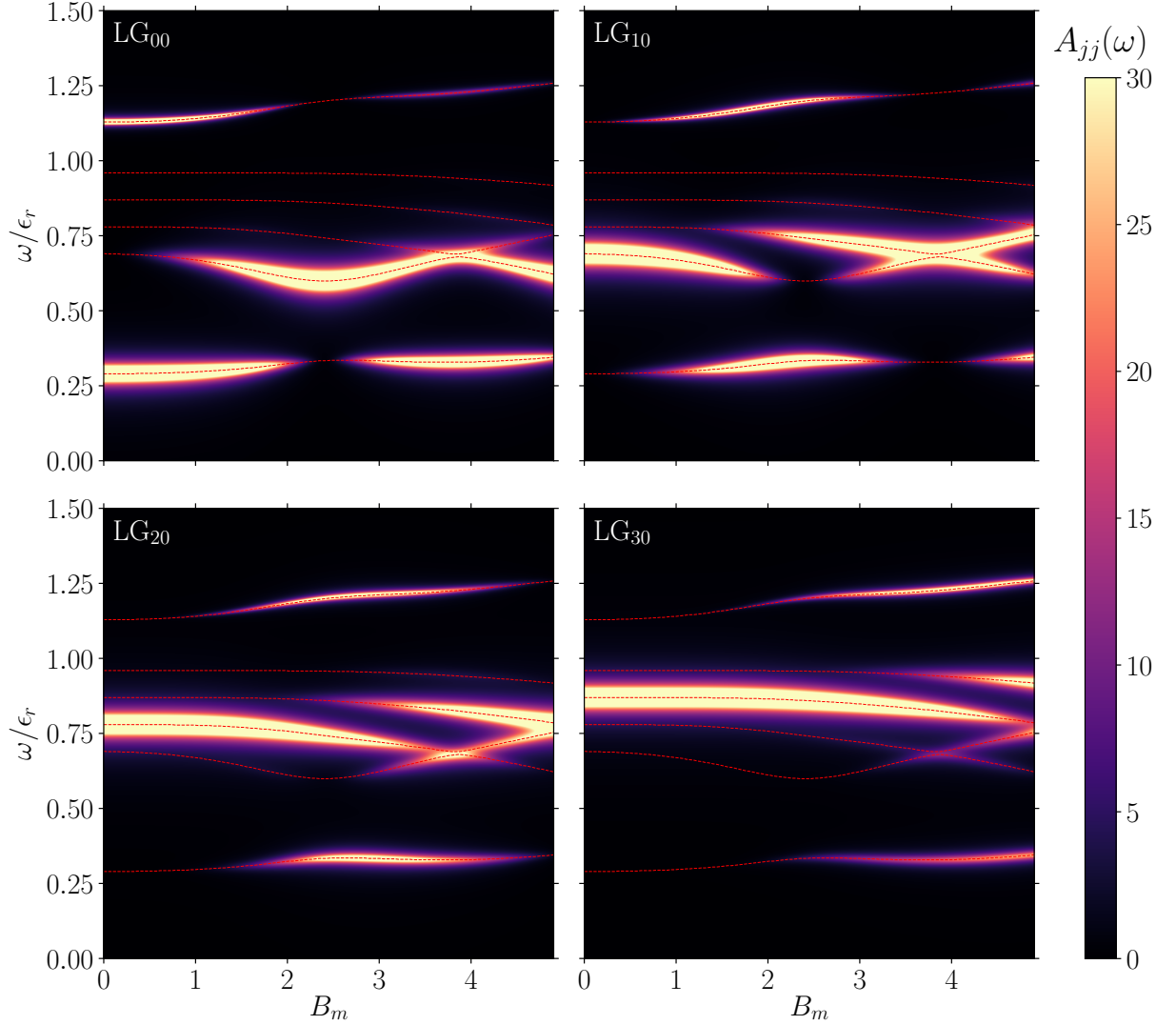


FIG. 6: Distribution of the spectral weight as a function of the modulation amplitude for different components of the cavity field, corresponding to the first four radial transverse modes LG_{pl} with $p \in \{0, 1, 2, 3\}$. The PM frequency is chosen such that the higher order modes have a large effective detuning ($\epsilon = -0.09\epsilon_R$) and $\Lambda^2 = 0.7\Lambda_c(B_m)^2$, with the renormalized coupling strength defined in Eq. (15). The zeroth mode has detuning $\Delta_0 = 0.6$, while the remaining parameters are as in Fig. 4. The red lines are poles of the real part of the cavity propagator in Eq. (11) and therefore indicate the polariton frequencies.

two peak structure discussed in Fig. 4 (a), whereas the higher-order modes have no atom peak in the spectrum but only their bare Lorentzian lineshape at the respective detunings. As B_m is increased the other modes start to couple through the atoms at the price of decreasing the atom coupling of the LG_{00} mode. This is clearly seen by the fact that the LG_{10} line starts showing up in A_{00} . Near $B_m \approx 2.3$, the coefficient c_0 vanishes, see Fig. 3. This means that the LG_{00} mode no longer couples to the atoms, and both the atom peak and what will become the superradiant peak vanish from A_{00} . At that modulation depth, A_{00} is simply the free Lorentzian line shape at Δ_0 . Meanwhile, both LG_{10} and LG_{20} couple relatively strongly to the atoms, and therefore effectively to each other, which introduces multiple peaks in the

corresponding components of the spectral function. Further increasing B_m reintroduces the LG_{00} mode in the polariton peaks.

This shows that one can tune B_m such that the polaritons have contributions from many modes. In particular, the polariton becoming unstable at the superradiant transition will then be a linear combination of all modes LG_{j0} with $j < \alpha_M$, with weights essentially given by the histograms in Fig. 5. As the higher modes have a larger detuning than the zeroth mode, it is necessary to increase the pump power in order to keep the ratio Λ/Λ_c fixed. This shows up in the spectral functions, where the atomic peak is pushed to higher energies as B_m is increased. It is interesting to note that, even though the higher-energy modes are red detuned, one can choose a

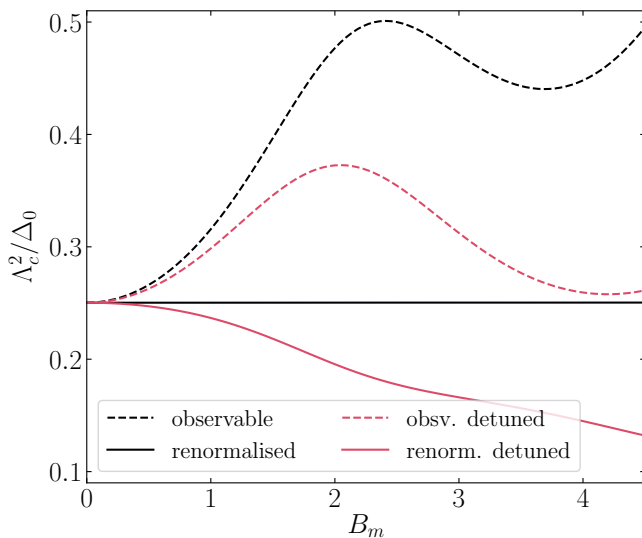


FIG. 7: Critical coupling strength Λ_c as a function of the modulation amplitude. The two different colors represent $\Omega = \omega_T$ (black) and an effective detuning between the modes $\Omega = \omega_T + 0.1$ (red). The remaining parameters are the same as the ones used in Fig. 6. The dashed lines are obtained for the same systems but with the critical coupling strength being renormalized to make up for the lost power in the unused laser sidebands given by Eq. (15).

modulation depth which results in anticrossings, especially prominent at around $B_m = 4$. This demonstrates that non-trivial multimode effects can be seen using both $\epsilon < 0$ and $\epsilon > 0$.

IV. MULTIMODE SUPERRADIANCE

Having multiple cavity modes available affects several features of the transition to the superradiant phase. The first clear effect is that the hybridization between multiple cavity modes can give rise to an increase in Λ_c compared to the unmodulated system, as seen in Fig. 6. The behaviour of Λ_c is plotted as a function of B_m in Fig. 7. To isolate the effect, consider first the case where $\Omega = \omega_T$. In this case all modes in the system have the same effective detuning. The value of Λ_c one would observe in an experiment is the black dashed line increasing non-monotonically as the PM is increased. This rise in the critical coupling strength is due to the PM being symmetric around the carrier frequency. The higher-order modes see only the closest laser sideband, but the PM also induces sidebands at a lower energy than the carrier frequency. For these negative frequency sidebands the cavity has no stable modes as they correspond to very high transverse quantum numbers with a lower longitudinal quantum number. These modes are lossy due to their large transverse size and are generally not stable. The power in the lower frequency peaks is therefore effectively lost. This means that the total effective pumping

power of the cavity is decreased by the weight in the negative frequency coefficients. This effect can be taken into account by renormalising the coupling

$$\Lambda^2 \rightarrow \frac{\Lambda^2}{\sum_{0 \leq \alpha < \alpha_M} c_\alpha^2} = \Lambda(B_m)^2. \quad (15)$$

We always use the explicit B_m dependence to denote the renormalized coupling strength. Employing this renormalization one sees that $\Lambda_c(B_m)$ stays constant through all modulation depths. When $\epsilon > 0$, as in Fig. 4 (b), the higher-order modes have a smaller detuning, and one again sees that Λ_c is increasing with B_m . This might seem counter-intuitive, as the higher modes have smaller effective detunings and one would therefore expect Λ_c to decrease with B_m , which is indeed observed when using the renormalized coupling strength.

Another important modification to single-mode superradiance is that with a positive ϵ , higher-order modes have a lower frequency than the zeroth mode. For a range of values of ϵ , B_m and Δ_0 , the situation arises where some higher-order modes are effectively red-detuned from their nearest sideband. In this case the magnitudes of their detunings are still small, compared to ω_T , but now have negative signs. For a single-mode system, this leads to an instability at a much smaller Λ_c than for a similarly blue-detuned cavity mode. The critical coupling is much smaller because the bare atomic part of the system has a vanishingly small loss and once the cavity is red detuned the atomic part of the system is easily rendered unstable, even at very weak interaction strengths. This type of “atomic instability” happens at finite frequency, that is, the atomic polariton becoming unstable still has a finite energy. This instability is thus of a very different nature than the superradiant transition happening at Λ_c , via a zero frequency excitation.

The results presented so far assume that the system remains stable up to Λ_c , which means that we have to choose the parameters such that the finite-frequency instability is avoided. Fig. 8 (a) shows the nature of the leading instability as a function of the PM parameters. For $\epsilon < 0.15$ the transition always happens to a stationary, superradiant phase. This is explained by the fact that we have considered a system with 5 available modes and with $\Delta_0 = 0.6$. This means that the smallest detuning for this region is $\Delta_4 = \Delta_0 - 4\epsilon \geq 0$, which does not allow for a finite-frequency instability. Clearly, the constraint on the number of cavity modes imposed by the physical setup plays an important role for the existence of the finite frequency instability. When moving to larger values of ϵ it can be seen that, due to the effective interactions between multimode polaritons, the boundary between zero- and finite-frequency instabilities is highly non-linear. For the parameters considered in the present work, there is thus a large region where the PM can be used to generate multimode Floquet polaritons without encountering a finite-frequency instability.

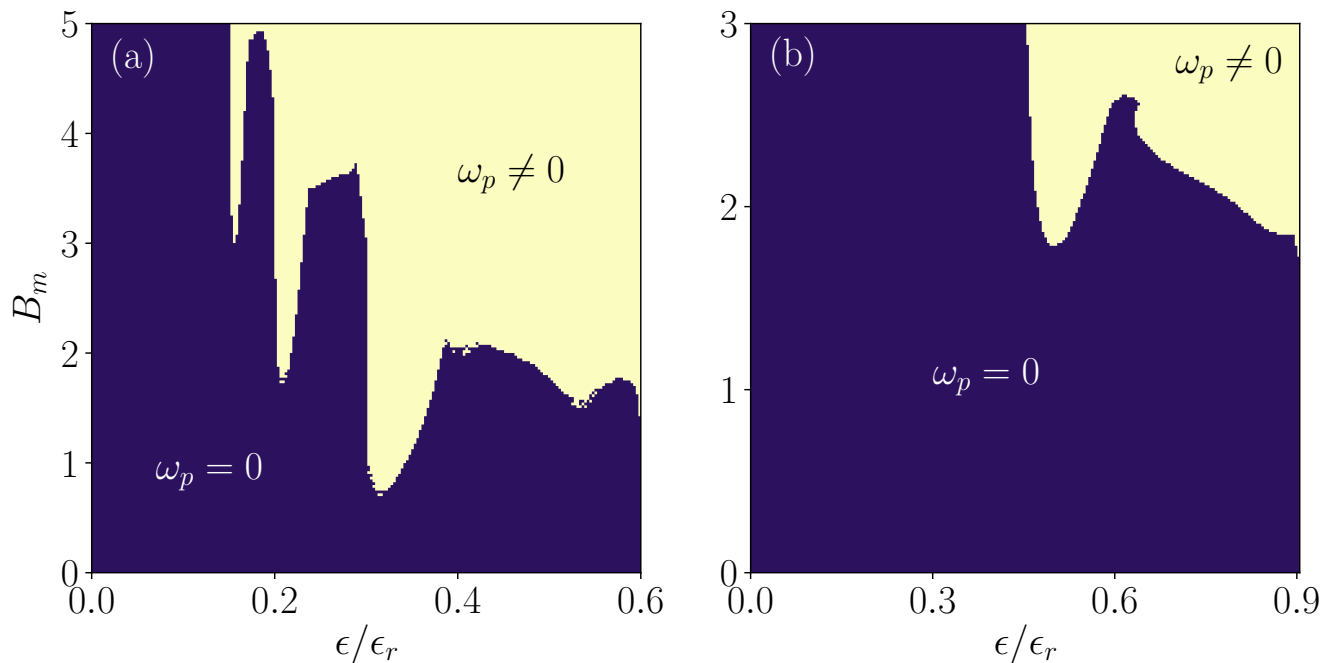


FIG. 8: Plot of the dominant instability of the system as a function of the PM parameters. In panel (a) we have chosen the same parameters as in Fig. 6 but with $\kappa = 0.05\epsilon_r$. In (b), we employed the parameters from the Hamburg experiment of reference [23]: $\kappa = 0.2\epsilon_r$, $w_0/Q = 244$, $L_H = w_0/10$, as well as a cavity detuning $\Delta_0 = 4.5\kappa$. In the blue region the system experiences a transition to a superradiant phase at the finite critical coupling strength Λ_c . The bright color indicates parameters where a finite-frequency instability takes place at $\Lambda < \Lambda_c$.

V. EXPERIMENTAL OBSERVABILITY

The scheme proposed here can be realized in several state-of-the-art laboratories. The main feature we discussed is the presence of anticrossings, which is a clear signature of the formation of the multimode Floquet polaritons. A prerequisite for achieving appreciable hybridization between different cavity modes, is that two resonances in the spectral function have to be brought close to each other. As all cavity modes have a positive detuning, the corresponding peaks move towards zero frequency when coupling to the atoms. In order to generate an (avoided) crossing, we therefore need to make a mode of higher energy move to zero faster than a lower-energy mode, while they both couple to the atoms. From the previous discussions it is clear that one way of achieving this is by having $\epsilon > 0$, such that there is a higher-order mode that has a smaller detuning. This was shown in Fig. 4 (b). By introducing a shallow PM, the zeroth mode will couple strongly to the atoms. This will push it faster towards zero than the higher-order mode which couples weaker to the atoms. As the zeroth mode comes close to the higher-order cavity mode, their repulsion will be determined by how strongly they effectively interact through the atoms. Similarly, one could use $\epsilon < 0$ in combination with a deeper modulation, as done in Fig. 6. Generating the strongest hybridization between the cavity modes is therefore a question of choosing the param-

eters such that the higher-energy mode moves faster but the lower-energy mode still couples significantly to the atoms.

To generate this scenario it is necessary to have cavity modes with detunings smaller than the recoil energy of the atoms. This is a significant constraint for experimental observability, as it means that the cavity loss rate has to be smaller than the recoil energy. The weaker the losses the sharper the avoided crossings that can be observed. Loss rates below the recoil energy can be obtained in long cavities without sacrificing strong light-matter interaction. Here the mode volume is small at the position of the atom cloud and the loss is kept small because of the long round trip distance of the cavity photon. Such a cavity system is for example used in Hamburg [23]. For the cavity geometry used in the experiment, the modes closest to each other in energy, and thus within the energy range of the PM photons, are not only different transverse modes but also possess different longitudinal mode numbers. This differs from the scenario so far described in this work. However, our suggested modulation scheme is highly adaptable and one can therefore choose a modulation frequency Ω that directly couples different transverse modes with the same longitudinal mode number by choosing $\Omega \sim V_{FSR} - \omega_T$. This is easily possible for the small free spectral range V_{FSR} of the long cavity in the Hamburg experiment, as it would require $\Omega \sim 2.4\text{GHz}$, which is well within the

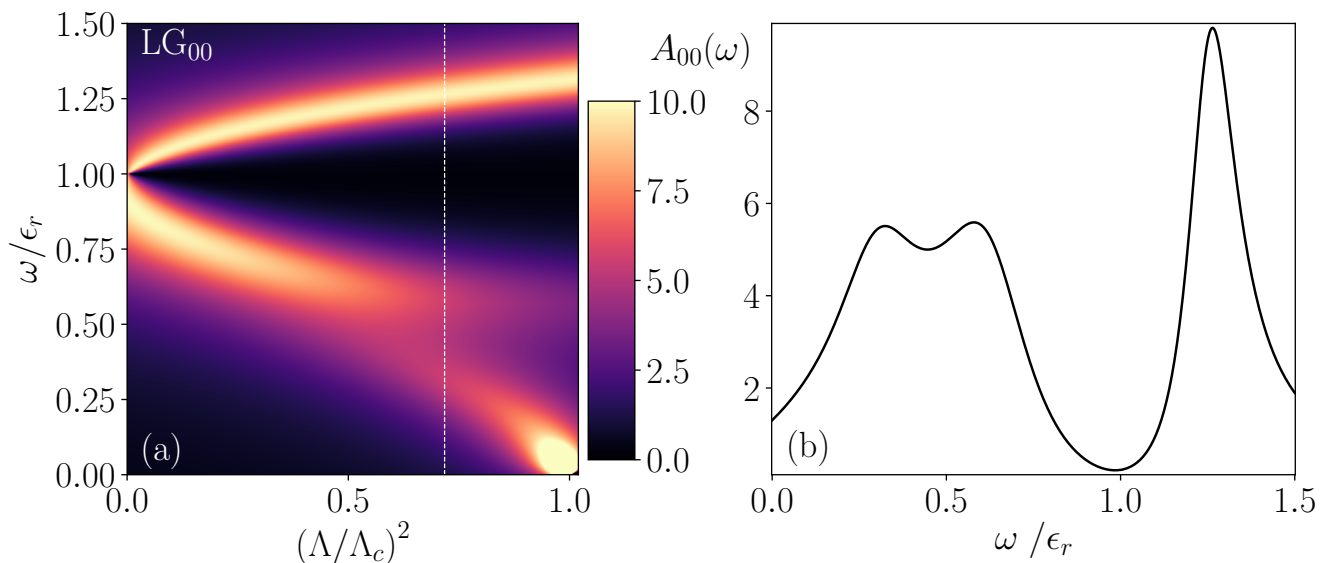


FIG. 9: Spectral function of LG_{00} mode for $B_m = 0.9$ and $\epsilon = 2\kappa$. b) Cut at the white dashed line shown in a). All other parameters are taken directly from the experimental setup used in Hamburg [23] given in Fig. 8 (b).

range of current fiber-based electro-optical modulators. In this experiment $\kappa/\epsilon_R \approx 0.2$, allowing for the subrecoil resolution necessary to see the described avoided crossings. We suggest to filter the cavity output for the LG_{00} mode and measure the distribution of the spectral weight. In Fig. 8 (b), we have seen that there is a large range of parameters available to adjust the PM while preserving a zero frequency superradiant instability at a finite coupling strength. Choosing PM parameters that allow an anticrossing for the experimental parameters of [23], our prediction is shown in Fig. 9. We see that an anticrossing is visible in the spectral weight of the LG_{00} component of the cavity field. In addition, clear multimodality should be observable by decomposing the cavity output light after entering the superradiant phase, as is typically done for degenerate cavities [28]. Differently from the avoided crossings, a multimodal cavity output should be visible even when the loss rate is much larger than the recoil energy.

VI. CONCLUSION

We have shown that the periodic phase modulation of the driving laser can generate a large dispersive coupling between an ultracold atomic cloud and many modes of a non-degenerate cavity. This leads to the formation of multimode Floquet polaritons. Their mutual interactions mediated by the atoms are visible as avoided crossings and ultimately lead to a phase transition to a multimode superradiant state. This scenario should be experimentally testable in state-of-the-art platforms.

In this investigation, we have focused on the energetic effect of the PM and simplified the degrees of freedom by

considering small atom clouds at the center of the cavity. Having seen that multimode Floquet polaritons can be generated, a very interesting aspect is to explore regimes where the cloud has significantly different overlaps with the different resonant modes. This allows one to establish an added competing effect that can further enrich the multimode correlations. Moreover, the multimode nature of the polaritons and their mutual interactions might give rise to a richer scenario for finite-frequency instabilities. We defer these studies to future work.

ACKNOWLEDGEMENT

We thank Alexander Baumgärtner, Tobias Donner, Davide Dreon, and Tilman Esslinger for useful discussions.

Appendix A: Mode overlaps

To calculate the density response, Eq. (8), one has to compute the overlaps between atom cloud, cavity and laser. In general these overlaps will have to be solved numerical but a closed form solution can be found when the atomic states are well described as eigenstates of the radially symmetric, harmonic trap. Furthermore, the laser form-factor η_p also has to be approximated as a constant. With a shallow longitudinal trap and if the atoms are in a zero-temperature BEC then the longitudinal part of the atom eigenstate is tightly localized in momentum space. This means that the longitudinal part of the overlap leads to the atoms scattering into a state with momentum Q , set by the cavity geometry. The transverse part of the

overlap can be computed both for centered and non-centered atom clouds. For the more general case when radial symmetry is broken, one finds that the integral over three Hermite polynomials leads to three finite sums

$$\langle \psi_0 | \eta_{j\alpha} | \psi_{n\beta} \rangle = \frac{1}{\pi L_H^2} \sqrt{\frac{j!n!}{(j+|\alpha|)!(n+|\beta|)!}} \int_0^{2\pi} d\theta \int_0^\infty dr r \exp[i\theta(\alpha - \beta) - r^2(L_H^{-2} + \frac{1}{2}w_0^{-2})] \\ \times \left(\frac{r}{L_H}\right)^{|\beta|} \left(\frac{r}{w_0}\right)^{|\alpha|} L_j^{|\alpha|} \left(\frac{r^2}{w_0^2}\right) L_n^{|\beta|} \left(\frac{r^2}{L_H^2}\right), \quad (\text{A1})$$

where the mode indices have been split into a radial mode index (roman letter) and an angular index (greek letter). The non-BEC scattering state in Eq. (8) leads to a decoupling of cavity modes with different angular index,

through the $\delta_{\alpha,\beta}$ from the angular integral. Starting in angular momentum zero we therefore consider only the states with zero angular momentum. The remaining radial integral then has a closed form solution given by

$$\langle \psi_0 | \eta_{j0} | \psi_{n0} \rangle = \langle \psi_{n0} | \eta_j | \psi_0 \rangle = \frac{\Gamma(j+n'+1)}{2^{n'} n'! j!} \frac{(\delta^2 - \frac{1}{2})^j}{(\delta^2 + \frac{1}{2})^{j+n'+1}} {}_2F_1 \left[-n', -j; -n' - j; -\frac{\delta^2 + \frac{1}{2}}{\delta^2 - \frac{1}{2}} \right], \quad (\text{A2})$$

where $\delta = w_0/L_H$ is the relative size of the cavity waist compared to the transverse harmonic trapping length, ${}_2F_1$ is the Gauss hypergeometric function and Γ the Gamma function. Clearly these overlaps are fully determined by the cavity waist and radially symmetric harmonic trap strength which sets L_H . The simplest

case is when the BEC is significantly narrower than the cavity waist. In this limit $\delta^2 \gg 1$ and therefore $\lim_{\delta \rightarrow \infty} \langle \psi_0 | \eta_{j0} | \psi_{n0} \rangle = \delta_{n0}$. In all presented calculations the result from Eq. (A2) has been used and the number of atomic states have been truncated only after convergence has been achieved.

-
- [1] Darrick E. Chang, Vladan Vuletić, and Mikhail D. Lukin. Quantum nonlinear optics —photon by photon. *Nature Photonics*, 8(9):685–694, 2014.
 - [2] H. J. Kimble. The quantum internet. *Nature*, 453(7198):1023–1030, 2008.
 - [3] Mark Saffman, Thad G Walker, and Klaus Mølmer. Quantum information with Rydberg atoms. *Reviews of modern physics*, 82(3):2313, 2010.
 - [4] Iacopo Carusotto and Cristiano Ciuti. Quantum fluids of light. *Reviews of Modern Physics*, 85(1):299, 2013.
 - [5] Changsuk Noh and Dimitris G Angelakis. Quantum simulations and many-body physics with light. *Reports on Progress in Physics*, 80(1):016401, Nov 2016.
 - [6] Michael Fleischhauer, Atac Imamoglu, and Jonathan P. Marangos. Electromagnetically induced transparency: Optics in coherent media. *Rev. Mod. Phys.*, 77:633–673, Jul 2005.
 - [7] Michael J Hartmann, Fernando GSL Brandao, and Martin B Plenio. Strongly interacting polaritons in coupled arrays of cavities. *Nature Physics*, 2(12):849–855, 2006.
 - [8] Alexey V Gorshkov, Rejish Nath, and Thomas Pohl. Dissipative many-body quantum optics in Rydberg media. *Physical review letters*, 110(15):153601, 2013.
 - [9] James S Douglas, Hessam Habibian, C-L Hung, Alexey V Gorshkov, H Jeff Kimble, and Darrick E Chang. Quantum many-body models with cold atoms coupled to photonic crystals. *Nature Photonics*, 9(5):326–331, 2015.
 - [10] James S Douglas, Tommaso Caneva, and Darrick E Chang. Photon molecules in atomic gases trapped near photonic crystal waveguides. *Physical Review X*, 6(3):031017, 2016.
 - [11] Stefan Ostermann, Francesco Piazza, and Helmut Ritsch. Spontaneous crystallization of light and ultracold atoms. *Physical Review X*, 6(2):021026, 2016.
 - [12] Emil Zeuthen, Michael J. Gullans, Mohammad F. Maghrebi, and Alexey V. Gorshkov. Correlated Photon Dynamics in Dissipative Rydberg Media. *Phys. Rev. Lett.*, 119:043602, Jul 2017.
 - [13] Kieran A Fraser and Francesco Piazza. Topological soliton-polaritons in 1D systems of light and fermionic matter. *Communications Physics*, 2(1):1–7, 2019.
 - [14] Ruichao Ma, Brendan Saxberg, Clai Owens, Nelson Leung, Yao Lu, Jonathan Simon, and David I Schuster. A dissipatively stabilized Mott insulator of photons. *Nature*, 566(7742):51–57, 2019.
 - [15] Johannes Lang, Darrick Chang, and Francesco Piazza.

- Interaction-induced transparency for strong-coupling polaritons. *Physical Review Letters*, 125(13):133604, 2020.
- [16] Ningyuan Jia, Nathan Schine, Alexandros Georgakopoulos, Albert Ryou, Logan W Clark, Ariel Sommer, and Jonathan Simon. A strongly interacting polaritonic quantum dot. *Nature Physics*, 14(6):550–554, 2018.
- [17] Nathan Schine, Albert Ryou, Andrey Gromov, Ariel Sommer, and Jonathan Simon. Synthetic Landau levels for photons. *Nature*, 534(7609):671–675, 2016.
- [18] Hyang-Tag Lim, Emre Togan, Martin Kroner, Javier Miguel-Sanchez, and Atac Imamoglu. Electrically tunable artificial gauge potential for polaritons. *Nature communications*, 8(1):1–6, 2017.
- [19] Li Bing Tan, Ovidiu Cotlet, Andrea Bergschneider, Richard Schmidt, Patrick Back, Yuya Shimazaki, Martin Kroner, and Atac Imamoglu. Interacting polaron-polaritons. *Physical Review X*, 10(2):021011, 2020.
- [20] A Goban, C-L Hung, S-P Yu, JD Hood, JA Muniz, JH Lee, MJ Martin, AC McClung, KS Choi, Darrick E Chang, et al. Atom–light interactions in photonic crystals. *Nature communications*, 5(1):1–9, 2014.
- [21] Logan W Clark, Ningyuan Jia, Nathan Schine, Claire Baum, Alexandros Georgakopoulos, and Jonathan Simon. Interacting floquet polaritons. *Nature*, 571(7766):532–536, 2019.
- [22] Kristian Baumann, Christine Guerlin, Ferdinand Brennecke, and Tilman Esslinger. Dicke quantum phase transition with a superfluid gas in an optical cavity. *Nature*, 464(7293):1301–1306, Apr 2010.
- [23] H. Keßler, J. Klinder, M. Wolke, and A. Hemmerich. Optomechanical atom-cavity interaction in the sub-recoil regime. *New Journal of Physics*, 16, 2014.
- [24] Päivi Törmä and William L Barnes. Strong coupling between surface plasmon polaritons and emitters: a review. *Reports on Progress in Physics*, 78(1):013901, 2014.
- [25] H. Keßler, J. Klinder, M. Wolke, and A. Hemmerich. Steering Matter Wave Superradiance with an Ultranarrow-Band Optical Cavity. *Physical Review Letters*, 113(7):070404, Aug 2014.
- [26] Jayson G. Cosme, Christoph Georges, Andreas Hemmerich, and Ludwig Mathey. Dynamical Control of Order in a Cavity-BEC System. *Physical Review Letters*, 121(15):153001, Oct 2018.
- [27] Hans Keßler, Jayson G Cosme, Christoph Georges, Ludwig Mathey, and Andreas Hemmerich. From a continuous to a discrete time crystal in a dissipative atom-cavity system. *New Journal of Physics*, 22(8):085002, 2020.
- [28] Alicia J. Kollár, Alexander T. Papageorge, Varun D. Vaidya, Yudan Guo, Jonathan Keeling, and Benjamin L. Lev. Supermode-density-wave-polariton condensation with a Bose–Einstein condensate in a multimode cavity. *Nature Communications*, 8(1):14386, Apr 2017.
- [29] Varun D. Vaidya, Yudan Guo, Ronen M. Kroeze, Kyle E. Ballantine, Alicia J. Kollár, Jonathan Keeling, and Benjamin L. Lev. Tunable-Range, Photon-Mediated Atomic Interactions in Multimode Cavity QED. *Physical Review X*, 8(1):011002, Jan 2018.
- [30] Yudan Guo, Ronen M. Kroeze, Varun D. Vaidya, Jonathan Keeling, and Benjamin L. Lev. Sign-Changing Photon-Mediated Atom Interactions in Multimode Cavity Quantum Electrodynamics. *Physical Review Letters*, 122(19):193601, May 2019.
- [31] Yudan Guo, Varun D. Vaidya, Ronen M. Kroeze, Rhannon A. Lunney, Benjamin L. Lev, and Jonathan Keeling. Emergent and broken symmetries of atomic self-organization arising from Gouy phase shifts in multimode cavity QED. *Physical Review A*, 99(5):053818, May 2019.
- [32] Sarang Gopalakrishnan, Benjamin L. Lev, and Paul M. Goldbart. Emergent crystallinity and frustration with Bose–Einstein condensates in multimode cavities. *Nature Physics*, 5(11):845–850, Nov 2009.
- [33] P Karpov and F Piazza. Crystalline droplets with emergent color charge in many-body systems with sign-changing interactions. *Physical Review A*, 100(6):61401, Dec 2019.
- [34] Daniel Adam Steck. Rubidium 87 Line Data. pages 1–29, 2009.
- [35] Christopher C. Gerry and Peter L. Knight. *Introductory Quantum Optics*. Cambridge University Press, 2005.
- [36] H.-P. Breuer and F. Petruccione. *The Theory of Open Quantum Systems*. Oxford University Press, page 625, 2007.
- [37] Francesco Piazza and Philipp Strack. Quantum kinetics of ultracold fermions coupled to an optical resonator. *Physical Review A - Atomic, Molecular, and Optical Physics*, 90(4), 2014.
- [38] Francesco Piazza, Philipp Strack, and Wilhelm Zwerger. Bose-Einstein condensation versus Dicke-Hepp-Lieb transition in an optical cavity. *Annals of Physics*, 339:135–159, 2013.
- [39] Johannes Lang, Darrick E Chang, and Francesco Piazza. Nonequilibrium diagrammatic approach to strongly interacting photons. *Physical Review A*, 102(3):033720, 2020.
- [40] G.S. Agarwal. *Quantum Optics*. Cambridge University Press, 2013.
- [41] A.L. Fetter and J.D. Walecka. *Quantum Theory of Many-particle Systems*. Dover Books on Physics. Dover Publications, 2003.
- [42] Anthony E Siegman. *Lasers*. University Science Books, 1986.
- [43] M. Abramowitz and I.A. Stegun. *Handbook of Mathematical Functions: With Formulas, Graphs, and Mathematical Tables*. Applied mathematics series. Dover Publications, 1965.
- [44] Emanuele G. Dalla Torre, Sebastian Diehl, Mikhail D. Lukin, Subir Sachdev, and Philipp Strack. Keldysh approach for nonequilibrium phase transitions in quantum optics: Beyond the Dicke model in optical cavities. *Phys. Rev. A*, 87:023831, Feb 2013.
- [45] D. Nagy, G. Szirmai, and P. Domokos. Self-organization of a Bose-Einstein condensate in an optical cavity. *European Physical Journal D*, 48(1):127–137, 2008.